# Variation of P-wave reflectivity with offset and azimuth in anisotropic media

Andreas Rüger
*Department of Geophysics*
*Center for Wave Phenomena*
*Colorado School of Mines, Golden, CO 80401, USA*

**ABSTRACT**
Recent results on symmetry-plane $P$-wave reflection coefficients in azimuthally anisotropic media are extended to observations at arbitrary azimuth, large incidence angles and to lower symmetry systems. The approach presented here is based on analysis of linearized reflection and transmission coefficients in azimuthally anisotropic media. The approximate $P$-wave reflection coefficient in transversely isotropic media with a horizontal axis of symmetry (HTI) (typical for a system of parallel vertical cracks embedded in an isotropic matrix) shows that the AVO gradient varies as a function of the squared cosine of the azimuthal angle. This change can be inverted for the symmetry-plane directions and a combination of the shear-wave splitting parameter $\gamma$ and the anisotropy coefficient $\delta^{(V)}$. The parameters $\gamma$ and $\delta^{(V)}$ cause the same functional form of azimuthal change of the AVO gradient and cannot be extracted individually.

Azimuthal variations in the reflection coefficient at large angles of incidence (greater than 20°) can serve as an indication of azimuthal anisotropy even if no azimuthal AVO-gradient change can be observed. In this case, the azimuthal variation of the reflection coefficient at large incidence angles is primarily dependent on the anisotropy coefficient $\epsilon^{(V)}$ (closely related to Thomsen's parameter $\epsilon$) and provides enough information to detect the two symmetry-plane directions.

The reflection coefficient study is also extended to media of orthorhombic symmetry which are believed to be more realistic models for fractured reservoirs. The study shows that the orthorhombic and HTI reflection coefficients are very similar and that the azimuthal variation in the orthorhombic $P$-wave reflection response is a function of the shear-wave splitting parameter $\gamma$ and two anisotropy parameters describing $P$-wave anisotropy for near-vertical propagation in the symmetry planes.

**Key words:** Reflection coefficients, $P$-wave AVO, azimuthal anisotropy

## Introduction

Fracturing and directional horizontal stress fields can cause azimuthal anisotropy in the subsurface. Knowledge of the direction of open fractures, the degree of fracturing and compartmentalization is critical in understanding the flow of fluids or gas through the reservoir and in making decisions on drilling locations and optimization of reservoir productivity.

Most upper-crustal media and many naturally fractured hydrocarbon reservoirs show azimuthal anisotropy of various types and strength (Crampin, 1985). The most simple, "first-order" model to describe azimuthal anisotropy is transverse isotropy with a horizontal axis of symmetry (HTI). The most common physical reason for a medium of HTI symmetry is a system of parallel penny-shaped vertical cracks embedded in an isotropic matrix (Thomsen, 1995). Any deviation from this model lowers the symmetry of the system. Media of orthorhombic symmetry that are believed to represent

more realistic, azimuthally anisotropic models can, for example, be caused by a combination of horizontal layering and vertically aligned cracks. Likewise, a system of two orthogonal but not necessary identical crack systems or two identical crack systems at oblique angle lead to orthorhombic symmetry (Winterstein, 1990). More general combinations of fracture systems yield monoclinic or triclinic symmetries.

While seismic signatures of compressional waves in transversely isotropic media with a vertical axis of symmetry (VTI) have been an active study area in the last decade, research on HTI media has been predominantly focused on the propagation of shear waves. Shear waves are very sensitive to the direction and amount of the fracturing and several algorithms [mainly through analysis of shear-wave birefringence (Alford, 1986; Thomsen, 1988)] are nowadays used to extract this information from multicomponent data (Martin & Davis, 1987; Lynn, 1995; Michelena, 1995). While much attention has been devoted to the study of shear-wave splitting in HTI models, the dependence of compressional wave data on the azimuthal anisotropy is much less understood and $P$-wave$^\star$ data are rarely used to directly detect and characterize fractured zones or "weak spots". Certainly, a method for the direct identification of fracturing using $P$-wave data would be highly beneficial. The exploration community has become very sophisticated in the processing and acquisition of $P$-wave data; additionally, compressional data generally have better quality and are cheaper as compared to shear-wave data.

Just recently, it became better known that $P$-wave AVO signatures are sensitive to fractures or cracks. Mallick and Frazer (1991), for example, show on synthetic data that the $P$-wave AVO response from a fractured layer is azimuthally dependent. Similar azimuthal variations in the $P$-wave reflection response have been observed on field data by Lynn et al. (1995) and Johnson (1995).

To elucidate the relation between the $P$-wave reflection coefficients and the medium parameters, Rüger (1996b) derived approximate reflection coefficients for the symmetry planes of HTI media. The reflection coefficient was hereby linearized with respect to the relative changes in isotropy parameters across the reflecting boundary and new anisotropy parameters $\epsilon^{(V)}$, $\delta^{(V)}$, and $\gamma^{(V)}$, similar to Thomsen's (1986) coefficients. Based on his results and a new exact description of normal-moveout velocities in HTI media (Tsvankin, 1996c), Rüger and Tsvankin (1995) proposed a new AVO algorithm to improve the characterization of fractured reservoirs using $P$-wave data.

This paper is a continuation of the work by Rüger (1996b). Specifically, the fracture-detection algorithm based on the symmetry-plane $P$-wave reflection coefficients shown in Rüger (1996b) can be extended to observations at arbitrary azimuth, to variations of reflection coefficients at large incidence angles and to lower symmetry systems. While the symmetry-plane coefficients describe the magnitude of azimuthal change and show how to relate it to the medium parameters, the newly derived expressions help to apply the fracture detection algorithm for any set of azimuths, and characterize the functional type of the azimuthal variation caused by the different anisotropy parameters.

A second extension investigates the reflection response in the vertical symmetry planes of orthorhombic media. Finally, for completeness and further reference, the full system of symmetry-plane reflection and transmission coefficients for pure modes in HTI media is given. Although scattering coefficients for converted modes have been derived as well, they are not shown here due to their algebraic complexity.

## Symmetry planes of HTI media: analogies and notation

HTI media have two vertical symmetry planes. The plane formed by the symmetry axis and the vertical is called the "symmetry-axis" plane (Rüger, 1996b; Tsvankin, 1996c), while the plane perpendicular to the symmetry axis is denoted the "isotropy" plane. If the HTI symmetry is caused by vertically aligned cracks, the isotropy plane coincides with the fracture plane.

The equivalence between HTI and VTI media is the key observation to derive the polarization vectors, the phase velocities and the approximate and exact reflection coefficient in the symmetry-axis plane: the Christoffel equation that in general differs for VTI and HTI media is *identical* for waves propagating in the symmetry-axis plane of HTI media and vertical symmetry planes of VTI models. Consequently, all equations describing kinematic properties and polarizations are identical for transversely isotropic media with vertical symmetry axis and the symmetry-axis plane of HTI media (Rüger, 1996b; Tsvankin, 1996c).

The observed analogy also leads to the introduction of a new set of dimensionless anisotropy parameters similar to Thomsen's (1986) coefficients. Specifically, HTI media are conveniently described by the vertical $P$-wave velocity $\alpha$, the vertical velocity of the shear wave polarized parallel to the isotropy plane $\beta\,(\doteq \beta^{\|})$, and three

$^\star$ I am omitting the qualifiers in "quasi $P$"-wave and "quasi $S$"-wave

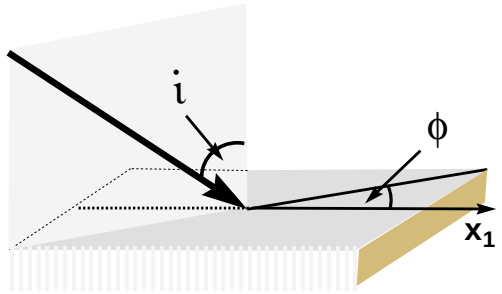


**Figure 1.** The incidence angle $i$ denotes the angle between the vertical and the slowness vector of the incident wave. The azimuthal angle $\phi$ is defined with respect to the symmetry axis pointing in the $x_1$-direction.

anisotropy parameters $\delta^{(V)}, \epsilon^{(V)}$ and $\gamma^{(V)}$. Anisotropy coefficients $\delta^{(V)}, \epsilon^{(V)}$ and $\gamma^{(V)}$ are Thomsen parameters defined with respect to vertical in the same way as in VTI media, i.e., they are different from the generic coefficients defined with respect to the horizontal symmetry axis. The set of new parameters naturally evolves from the analysis of the Christoffel system. Additionally, they represent the effective parameters describing the seismic signatures in HTI media. For example, $\alpha$ is the normal-moveout velocity recovered from seismic surveys aligned with the isotropy plane; $\delta^{(V)}$, on the other hand, determines the difference between the NMO velocity in this plane and in the symmetry-axis plane (Tsvankin, 1996c).

In some contexts, it is convenient to additionally use $\beta^{\perp}$, the slow vertical shear-wave velocity and the symmetry-axis velocities $V_{\rm P0}$ and $V_{\rm S0}$. Table 1 summarizes the coefficients used in the paper and relates them to the generic Thomsen parameters. Also included in this table is Thomsen's parameter $\gamma$ that is directly related to $\gamma^{(V)}$, the $\gamma$-parameter of the equivalent VTI model. The former is chosen in the parameterization of the reflection coefficients below because of its importance in the classical shear-wave splitting analysis.

## Approximate scattering coefficients for HTI media

The continuity of displacement and traction between elastic layers in welded contact leads to a system of equations that can be inverted for the reflection and transmission coefficients. The forward problem thus consists in solving a system of two, four or six boundary conditions, depending on the symmetry and the number of the wave modes above and below a reflecting interface. The inverse problem of estimating medium parameters from the angular changes of the reflection response represents a much more difficult problem. Koefoed (1955) went through the laborious exercise of numerically investigating reflection coefficients for many different sets of elastic, isotropic parameters. Obviously, extending this approach to azimuthally anisotropic media is not feasible. Instead, it is more helpful to derive approximate scattering coefficients (Bortfeld, 1961; Richards & Frasier, 1976; Aki & Richards, 1980; Banik, 1987; Thomsen, 1993; Ursin & Haugen, 1996) and learn about the influence of the anisotropy parameters on the reflection response.

The derivation of $P$-wave reflection coefficients in azimuthally anisotropic media involves the study of six wave modes generated by the incident $P$-wave. Probably the first results on this topic has been performed (but not explicitly published) by Corrigan (1990), who investigated the small-angle response at isotropic/orthorhombic boundaries. Using a Born-scattering approach, he derived the dependence of the initial slope of the reflection coefficient (also denoted as AVO gradient) $B$ on source-receiver azimuth of the form

$$B = B^{(0)} + B^{(1)} \cos 2\phi \,, \tag{1}$$

consistent with observations on synthetic data by Mallick (1991; 1995).

To verify and extend Corrigan's result to interfaces between two HTI media and higher angular terms, I used a perturbation technique similar to that applied by Thomsen (1993) for (azimuthally isotropic) VTI media. This approach considers a perturbation from an isotropic background medium and requires analytic expressions for $P$-wave polarization vectors, phase velocities and vertical slownesses as functions of the incidence phase angle $i$ and azimuthal phase angle $\phi$ (Figure 1) for weakly anisotropic HTI media.

A derivation of the polarization vectors without investigating the eigenvector problem of the HTI Christoffel matrix is shown in Appendix A. It only requires to apply the analogy of HTI and VTI media and some basic geometry to show that the $P$-wave polarization vector $\hat{\rm d}$ in HTI media can be expressed through the incidence phase angle and azimuthal phase angle as

$$\hat{\rm d}(i,\phi) = \begin{pmatrix} {\rm l}(i,\phi)\, \sin i\, \cos\phi \\ {\rm m}(i,\phi)\, \sin i\, \sin\phi \\ {\rm m}(i,\phi)\, \cos i \end{pmatrix} , \tag{2}$$

where m and l are given as

$$\begin{aligned} {\rm m}(i,\phi) &= 1 - f \sin^2 i \cos^2\phi \times \\ &\quad [\delta^{(V)} + 2(\epsilon^{(V)} - \delta^{(V)}) \sin^2 i \cos^2\phi] \\ {\rm l}(i,\phi) &= 1 + f\,(1 - \sin^2 i \cos^2\phi) \times \\ &\quad [\delta^{(V)} + 2(\epsilon^{(V)} - \delta^{(V)}) \sin^2 i \cos^2\phi] \,, \end{aligned} \tag{3}$$

with $f = \alpha^2/(\alpha^2 - \beta^2)$.

Phase velocities in HTI media as function of the angle with the symmetry axis and $\epsilon^{(V)}$ and $\delta^{(V)}$ are given

| | $c_{ij}$ – notation | generic Thomsen notation (exact) | (weak-anisotropy) |
|---|---|---|---|
| $\alpha$ | $\sqrt{c_{33}/\rho}$ | $V_{P0}\sqrt{1+2\epsilon}$ | $V_{P0}(1+\epsilon)$ |
| $\beta$ | $\sqrt{c_{44}/\rho}$ | $V_{S0}\sqrt{1+2\gamma}$ | $V_{S0}(1+\gamma)$ |
| $\beta^{\perp}$ | $\sqrt{c_{55}/\rho}$ | $V_{S0}$ | $V_{S0}$ |
| $\delta^{(V)}$ | $\frac{(c_{13}+c_{55})^2-(c_{33}-c_{55})^2}{2c_{33}(c_{33}-c_{55})}$ | $\frac{\delta-2\epsilon(1+\epsilon/f)}{(1+2\epsilon)(1+2\epsilon/f)}$ | $\delta-2\epsilon$ |
| $\epsilon^{(V)}$ | $\frac{c_{11}-c_{33}}{2c_{33}}$ | $-\frac{\epsilon}{1+2\epsilon}$ | $-\epsilon$ |
| $\gamma^{(V)}$ | $\frac{c_{66}-c_{44}}{2c_{44}}$ | $-\frac{\gamma}{1+2\gamma}$ | $-\gamma$ |
| $\gamma$ | $\frac{c_{44}-c_{66}}{2c_{66}}$ | $\gamma$ | $\gamma$ |

**Table 1.** Anisotropy parameters used to study HTI media and their relation to the generic Thomsen parameters. The $c_{ij}$ representation assumes that the symmetry axis is pointing in the $x_1$-direction. Parameter $f$ in the equation for $\delta^{(V)}$ is given by $f = 1 - V_{S0}^2/V_{P0}^2$.

in Tsvankin (1996c). Expressed using incidence and azimuthal angle, the $P$-wave phase velocity for weak anisotropy yields:

$$V_{P0}(i,\phi) = \alpha\left[1 + \delta^{(V)}\sin^2 i\cos^2\phi + (\epsilon^{(V)} - \delta^{(V)})\sin^4 i\cos^4\phi\right]. \quad (4)$$

Knowledge of the polarizations and phase velocities allows us to set up the perturbation equations for the reflection and transmission coefficients of the waves scattered at HTI/HTI interfaces with the same orientation of the symmetry axis above and below the interface. From the derivation shown in Appendix B, it follows that the compressional plane-wave reflection coefficient has the following dependence on the incidence (polar) and azimuthal phase angles:

$$R_P(i,\phi) = \frac{1}{2}\frac{\triangle Z}{\bar{Z}} + \frac{1}{2}\left\{\frac{\triangle\alpha}{\bar{\alpha}} - \left(\frac{2\bar{\beta}}{\bar{\alpha}}\right)^2\frac{\triangle G}{\bar{G}} + \left[\triangle\delta^{(V)} + 2\left(\frac{2\bar{\beta}}{\bar{\alpha}}\right)^2\triangle\gamma\right]\cos^2\phi\right\}\sin^2 i + \frac{1}{2}\left\{\frac{\triangle\alpha}{\bar{\alpha}} + \triangle\epsilon^{(V)}\cos^4\phi + \triangle\delta^{(V)}\sin^2\phi\cos^2\phi\right\}\times \sin^2 i\tan^2 i\,, \quad (5)$$

where $Z = \rho\alpha$ is the vertical $P$-wave impedance and $G = \rho\beta^2$ denotes the vertical shear modulus. The changes in the elastic parameters are expressed as relative differences. The vertical $P$-wave velocities in the upper and lower layer, for example, can be written as functions of the average velocity $\bar{\alpha} = 1/2\,(\alpha_2+\alpha_1)$ and the difference $\triangle\alpha = \alpha_2 - \alpha_1$:

$$\alpha_1 = \bar{\alpha}\,(1 - \frac{1}{2}\frac{\triangle\alpha}{\bar{\alpha}})\,,$$
$$\alpha_2 = \bar{\alpha}\,(1 + \frac{1}{2}\frac{\triangle\alpha}{\bar{\alpha}})\,.$$

Corresponding expressions are defined for the shear modulus, the density and the $P$-wave impedance.

The simplicity of approximation (5) is striking, especially because no angular terms have been neglected; simple trigonometrical relations describe the anisotropic contribution as a function of azimuth. For azimuth $\phi = 90^{\circ}$, equation (5) reduces to the approximate reflection coefficient for the isotropy plane in HTI media (Rüger, 1996b):

$$R_P(i,\pi/2) = \frac{1}{2}\frac{\triangle Z}{\bar{Z}} + \frac{1}{2}\left\{\frac{\triangle\alpha}{\bar{\alpha}} - \left(\frac{2\bar{\beta}}{\bar{\alpha}}\right)^2\frac{\triangle G}{\bar{G}}\right\}\sin^2 i + \frac{1}{2}\frac{\triangle\alpha}{\bar{\alpha}}\sin^2 i\tan^2 i\,. \quad (6)$$

The velocities of waves propagating in the isotropy plane are angle-independent and $R_P(i,\pi/2)$ has the same form as the isotropic approximation implied by Wright (1986) and first published by Thomsen (1990). As the other approximations used in this study, equation (6) is linearized in small relative differences (a useful assumption in many exploration contexts) and it is usually accurate enough for incidence angles not too close to the critical angle. Most importantly, it tells us what parameter combinations can be inverted for by investigating the intercept, gradient and higher angle terms of the reflection coefficient and hence forms the basis of conventional (isotropic) AVO analysis.

For the second vertical symmetry plane (the symmetry-axis plane) at azimuth $\phi = 0$, the linearized reflection coefficient has the following form:

$$R_P(i,0) = \frac{1}{2}\frac{\triangle Z}{\bar{Z}} + \frac{1}{2}\left\{\frac{\triangle\alpha}{\bar{\alpha}} - \left(\frac{2\bar{\beta}}{\bar{\alpha}}\right)^2\left(\frac{\triangle G}{\bar{G}} - 2\triangle\gamma\right) + \triangle\delta^{(V)}\right\}\sin^2 i +$$

$$\frac{1}{2}\left(\frac{\triangle\alpha}{\bar{\alpha}}+\triangle\epsilon^{(V)}\right)\sin^2 i\tan^2 i\ . \qquad (7)$$

As mentioned above, the same result can be derived by taking the known VTI approximate reflection coefficient and exploiting the analogy between VTI and HTI media. Comparing expressions (6) and (7) leads to the observation that the AVO-gradient term is varying between the isotropy plane and the symmetry-axis plane and that the difference in the shear-wave splitting parameter and the coefficient $\delta^{(V)}$ determine the magnitude of this variation (Rüger, 1996b; Rüger & Tsvankin, 1995). Similar observations can be made by investigating the symmetry-plane shear-wave reflection response in azimuthally anisotropic media. Symmetry-plane shear-wave reflection and transmission coefficients for HTI media have been used to study the viability of shear-wave AVO (Yardley & Crampin, 1991; Rüger, 1996a) and are included, for completeness, in Appendix C.

This paper is primarily focused on the azimuthal dependence of the reflection coefficient. Before studying equation (5) in more detail, it is instructive to first compare some numerically computed exact reflection coefficients with their linearized approximations. Hereby, it is not of most importance to achieve a high numerical accuracy (in that case, more complicated approximations such as those shown in Ursin and Haugen (1996) should be used), but to see if the simple analytic approximation (5) of an otherwise incomprehensibly complex reflection coefficient helps to quickly analyze the influence of anisotropy on the reflection signature. Equation (5) is linearized in nine small quantities $\frac{\triangle\alpha}{\bar{\alpha}}$, $\frac{\triangle Z}{\bar{Z}}$, etc. A total of 45 unknown quadratic terms are dropped in the derivation and it is not clear how the accuracy of the approximation depends on the medium parameters. In particular, it is of great interest to study the accuracy of equation (5) for different values of the anisotropy parameters $\epsilon^{(V)}$, $\delta^{(V)}$ and $\gamma$. Figure 2 shows the reflection coefficients evaluated at boundaries between isotropic and HTI media for azimuths of $0^\circ, 30^\circ, 60^\circ$ and $90^\circ$ and incidence angles up to 40 degrees. The parameters of the models used in this test are listed in Table 2. To perform a representative test of equation (5) and to study the sensitivity of the approximation with respect to the individual parameters, most examples shown use only one nonzero anisotropic parameter. This is done for test purposes only; in general, the anisotropy coefficients $\epsilon^{(V)}$, $\delta^{(V)}$ and $\gamma$ are not independent if the anisotropy is caused by vertical cracks.

The first test shown in Figure 2a corresponds to a reflecting HTI medium with a 10% shear-wave splitting parameter. The exact solutions (solid lines with decreasing thickness away from the symmetry-axis plane) and the approximations (dashed) are in very good agreement

| | $\frac{\triangle\alpha}{\bar{\alpha}}$ | $\frac{\triangle Z}{\bar{Z}}$ | $\frac{\triangle G}{\bar{G}}$ | $\delta^{(V)}$ | $\epsilon^{(V)}$ | $\gamma$ |
|---|---|---|---|---|---|---|
| Model a | 0.1 | 0.1 | 0.2 | 0 | 0 | 0.1 |
| Model b | 0.1 | 0.1 | 0.2 | -0.1 | 0 | 0 |
| Model c | 0.1 | 0.1 | 0.2 | 0 | -0.1 | 0 |
| Model d | 0.1 | 0.1 | 0.2 | -0.05 | -0.05 | 0.15 |

**Table 2.** Models used to test the accuracy of equation (5) and the sensitivity of the approximate reflection coefficients. The upper medium is isotropic, the lower medium has the following isotropic parameters: compressional vertical velocity $\alpha_2 = 2.5$, faster shear-wave vertical velocity $\beta_2 = 1.5$ and density $\rho_2 = 2.7$.

for all azimuths. The approximations practically coincide with the exact curves for $0^\circ$ and $30^\circ$ azimuths with the symmetry axis, while a small deviation is visible for azimuths $60^\circ$ and $90^\circ$ and large incidence angles. The second model has a nonzero coefficient $\delta^{(V)}$ in the reflecting medium. Equation (5) correctly predicts the split of the reflection coefficient curves. The slope of the exact curves for $0^\circ$ and $30^\circ$ azimuths is slightly overcorrected by the approximation and leads to deviations for large angles of incidence. Model c has a nonzero value of parameter $\epsilon^{(V)}$. According to equation (5), there should be no significant change in the AVO gradient (incidence angles $< 20^\circ$) and indeed, the exact solution does not show any split in the reflection coefficient curves for low angles of incidence. Note that inaccuracies for $0^\circ$ and $30^\circ$ azimuths are smaller than for $90^\circ$ azimuth. The latter approximation coincides with the classical isotropic linearization of the reflection coefficient that is used sucessfully in conventional AVO analysis. Therefore, in this case, the accuracy of the anisotropic approximation is higher than that for the isotropic one. Model d has three nonzero anisotropy parameters, including a shear-wave splitting coefficient of 15%. The accuracy of the approximation is acceptable for small values of incidence angles and also shows the correct trend for higher incidence angles. Deviations for large angles of incidence and $0^\circ$ and $30^\circ$ azimuths are caused by the approximation of shear-wave velocity $\beta^\perp$ through $\beta$ and $\gamma$ and hence are caused by the design of the approximation. For a better accuracy at small azimuths, the approximation (5) should be rewritten in terms of $\beta^\perp$.

## Functional type of the azimuthal variation

Rather than simply studying the reflection coefficient as a function of the incidence angle for several azimuths, equation (5) additionally suggests to fix the incidence

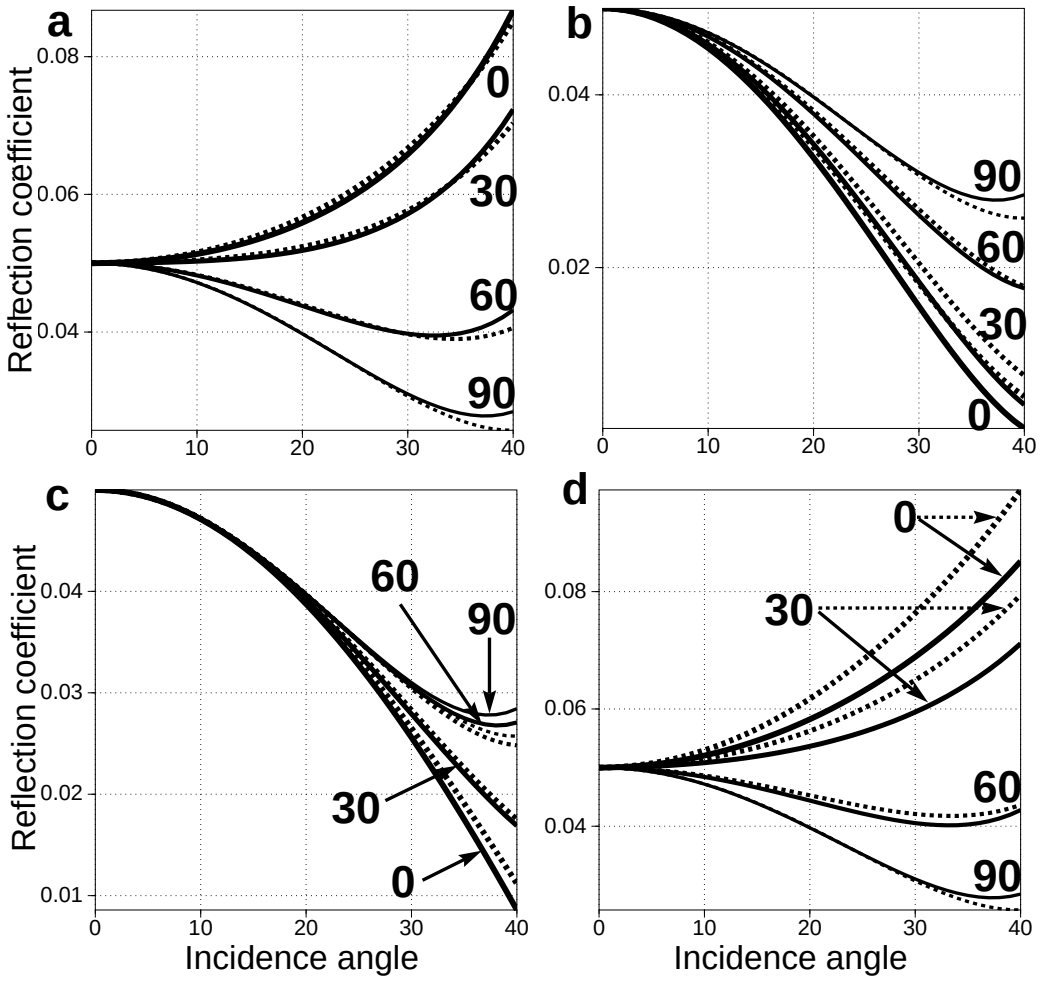


**Figure 2.** Reflection coefficients for an isotropic layer overlying an HTI medium. Shown are the exact solution (solid lines) and the weak elastic, weak anisotropic approximation (dashed) [equation (5)] for 0°, 30°, 60° and 90° azimuth. Table 2 lists the model parameters.

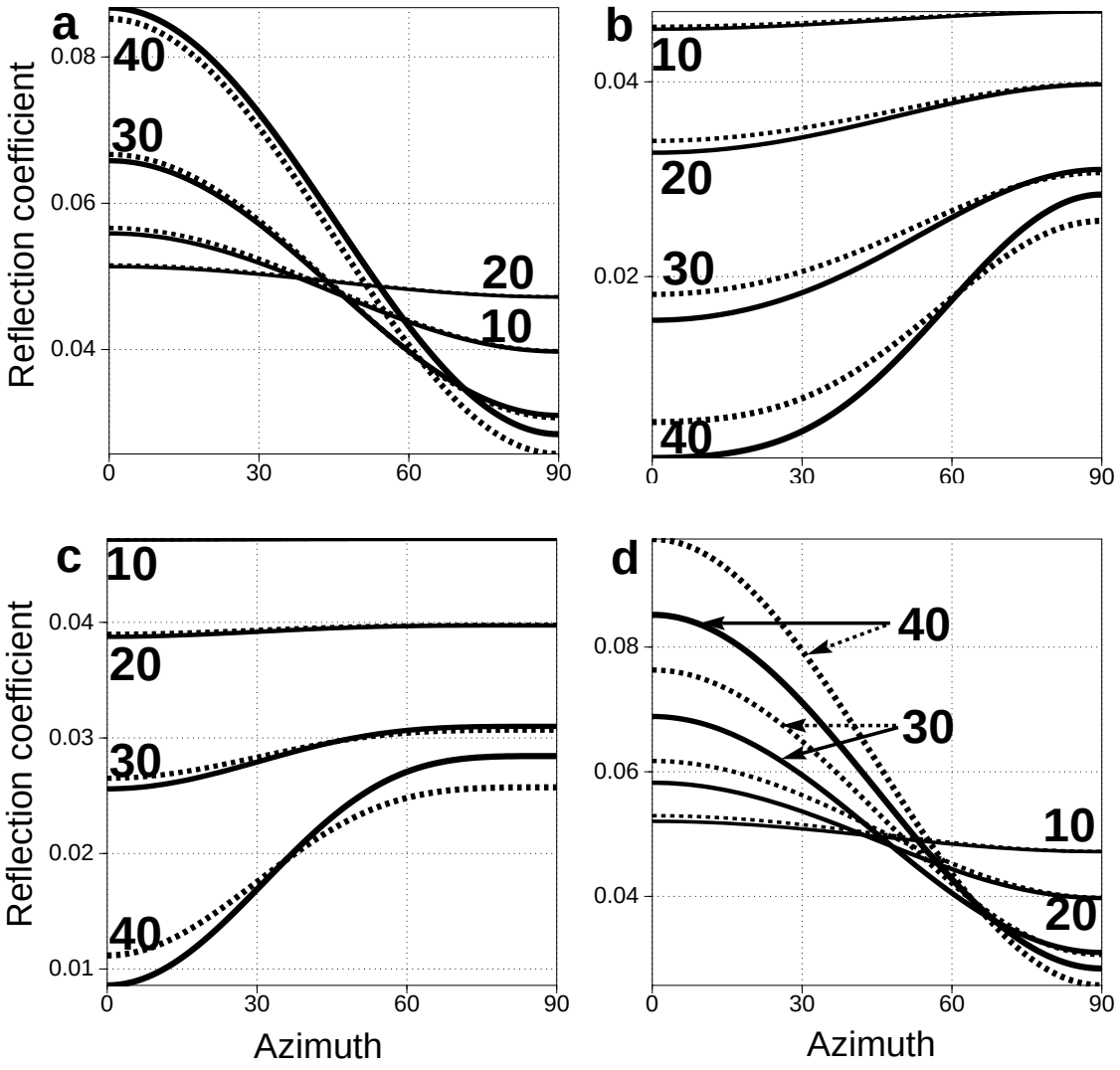


**Figure 3.** Reflection coefficients for an isotropic layer overlying an HTI medium as a function of the azimuthal phase angle. Shown are the exact solution (solid lines) and the weak elastic, weak anisotropic approximation (dashed) [equation (5)] for 10°, 20°, 30° and 40° incidence angle. Table 2 lists the model parameters.

angle and analyze the reflection coefficient as a function of azimuth. These curves are shown in Figure 3, for the models given in Table 2. The exact reflection coefficients are shown as solid lines for $10°, 20°, 30°$ and $40°$ incidence angles while the approximations are shown as dashed curves. Clearly, the approximations are very accurate for all azimuths and 10° and 20° incidence angles. For higher angles, the approximations start to deviate from the exact result, but correctly predict the functional type of the azimuthal change. Specifically, observing the azimuthal change of reflection coefficients for a fixed incidence phase angle clearly shows that the symmetry-plane directions at 0° and 90° azimuth coincides with the extrema of the reflection-coefficient curves.

Study of azimuthal changes of reflection coefficients such as shown in Figure 3 can help to find the orientation of the natural coordinate system of the subsurface without any prior knowledge of the medium parameters. Moreover, because the location of the extrema is the same for all incidence angles, the analysis of stacked data for several azimuths is enough to invert for the symmetry-plane directions, provided that the stack is performed with the proper (azimuthally varying) normal-moveout velocity. Amplitude analysis on stacked data, however, is not sufficient to decide which azimuth corresponds to the

symmetry-axis plane and which to the isotropy plane. For example, the maximum of the reflection curves occurs at 0° azimuth in Model a, while it is located at 90° azimuth in Model b.

The curves generated for Model c show several features that are not observed for the other examples. First, no azimuthal variation in the reflection coefficient is visible for 10° incidence angle and only a very slight variation at 20° incidence angle. Additionally, the functional type of the variation is different for large angles of incidence. As predicted by the $\cos^4\phi$ term in equation (5), the anisotropic part of the reflection coefficient rapidly decays away from the symmetry-axis plane while the azimuthal change is much less pronounced close to the isotropy-plane (Figure 6). As for the other examples, while the high-incidence-angle approximations start to deviate from the exact solution, the functional type of the azimuthal variation is nonetheless accurately approximated.

This discussion of the amplitude variations with offset and azimuth is still primarily qualitative. To relate the observed changes more closely to the medium parameters, let us now consider the implications of equation (5) to AVO-with-azimuth analysis.

Studies on AVO inversions based on the symmetry-plane coefficients (6) and (7) in Rüger and Tsvankin (1995) did not make use of the smooth azimuthal variation of the gradient and higher-angle ($\sin^2 i \tan^2 i$) terms between the two vertical symmetry planes. Moreover, while it is clear that $\Delta\gamma$ and $\Delta\delta^{(V)}$ are responsible for the magnitude of the azimuthal variation, it has not been obvious whether both coefficients cause a different rate of azimuthal change and hence can be inverted separately. Finally, in situations with small or non-existing AVO gradient variations, it is uncertain if the higher-angle term provides usable and extractable information about the subsurface. Below, I will use equation (5) to elucidate the character of the azimuthally varying reflection coefficient and discuss the feasibility of parameter estimation from variations of the AVO gradient and the higher-angle reflection amplitudes.

### The AVO gradient term

Equation (5) shows that azimuthal anisotropy in HTI media causes a different azimuthal dependence for the AVO gradient and the higher-angle term.

Small angular variations of $R_P(i,\phi)$ are described by the AVO gradient $B$ composed of the azimuthally invariant part $B^{\rm iso}$ and the anisotropic contribution $B^{\rm ani}$ multiplied with the squared cosine of the azimuthal angle $\phi$ with the symmetry axis. If the symmetry-axis orientation is unknown, $\phi$ should be formally expressed by the difference between the azimuthal direction $\phi_k$ of the $k-th$ observed azimuth and the direction of the symmetry-axis plane $\phi_{\rm sym}$. The AVO gradient measured at azimuth $\phi_k$ thus can be written as

$$B(\phi_k) = B^{\rm iso} + B^{\rm ani}\cos^2(\phi_k - \phi_{\rm sym}). \qquad (8)$$

This equation is nonlinear with three unknowns ($B^{\rm iso}$, $B^{\rm ani}$ and $\phi_{\rm sym}$). If the direction of the symmetry axis is known (for example from $S$-wave surveys), the equation becomes linear and two independent measurements suffice to solve for $B^{\rm iso}$ and $B^{\rm ani}$. The special case of inverting AVO measurements in the isotropy and symmetry-axis planes has been discussed in Rüger and Tsvankin (1995). In more realistic settings with noisy data, many more azimuths should be sampled and a least-squares approach could be used to find the optimum values of the unknowns in equation (8). Due to the nonlinearity of equation (8), the solution will not be unique and will yield a set of two orthogonal symmetry-plane orientations. However, a simple rough estimate of the sign of $B^{\rm ani}$ or a-priori knowledge of the approximate symmetry-axis direction is enough to identify which direction corresponds to the the isotropy and the symmetry-axis plane.

If $B(\phi_k)$ is known for several $\phi_k$'s, a graphical approach to determine the symmetry-plane directions and the magnitude of the variations can be used. If $B$ is plotted as a function of $\phi_k$, the locations of the extrema correspond exactly with the symmetry-plane orientations at 0° and 90° azimuth (and multiples of 90°). The values of B at the extrema yield estimates of $B^{\rm iso}$ and ($B^{\rm iso}$+$B^{\rm ani}$).

The dashed lines in Figure 4 shows the approximate AVO gradient based on equation (8). The "exact" gradient (solid line) is computed by simply averaging the slopes of the exact reflection coefficients for the first 20° incidence angles. Limiting the analysis to a smaller range of incidence angles would have produced a better match between the two curves, but it is unlikely that enough traces are available within this small angular range in a field data example. The curves shown in Figure 4 are evaluated for the models shown in Table 2. The extrema denoting the symmetry-plane directions can be easily picked, even though a-priory information is needed to distinguish between the symmetry-axis and the isotropy plane. Table 3 compares the magnitude of the observed AVO-gradient change with the the value of

$$B^{\rm ani} = 1/2\left[\Delta\delta^{(V)} + 2\left(\frac{2\bar{\beta}}{\bar{\alpha}}\right)^2\Delta\gamma\right], \qquad (9)$$

that would be obtained using equation (5).

Let us now assume that the solid curve is observed in a field experiment and that geologic data indicates that 0° and 90° azimuth corresponds to the symmetry-axis

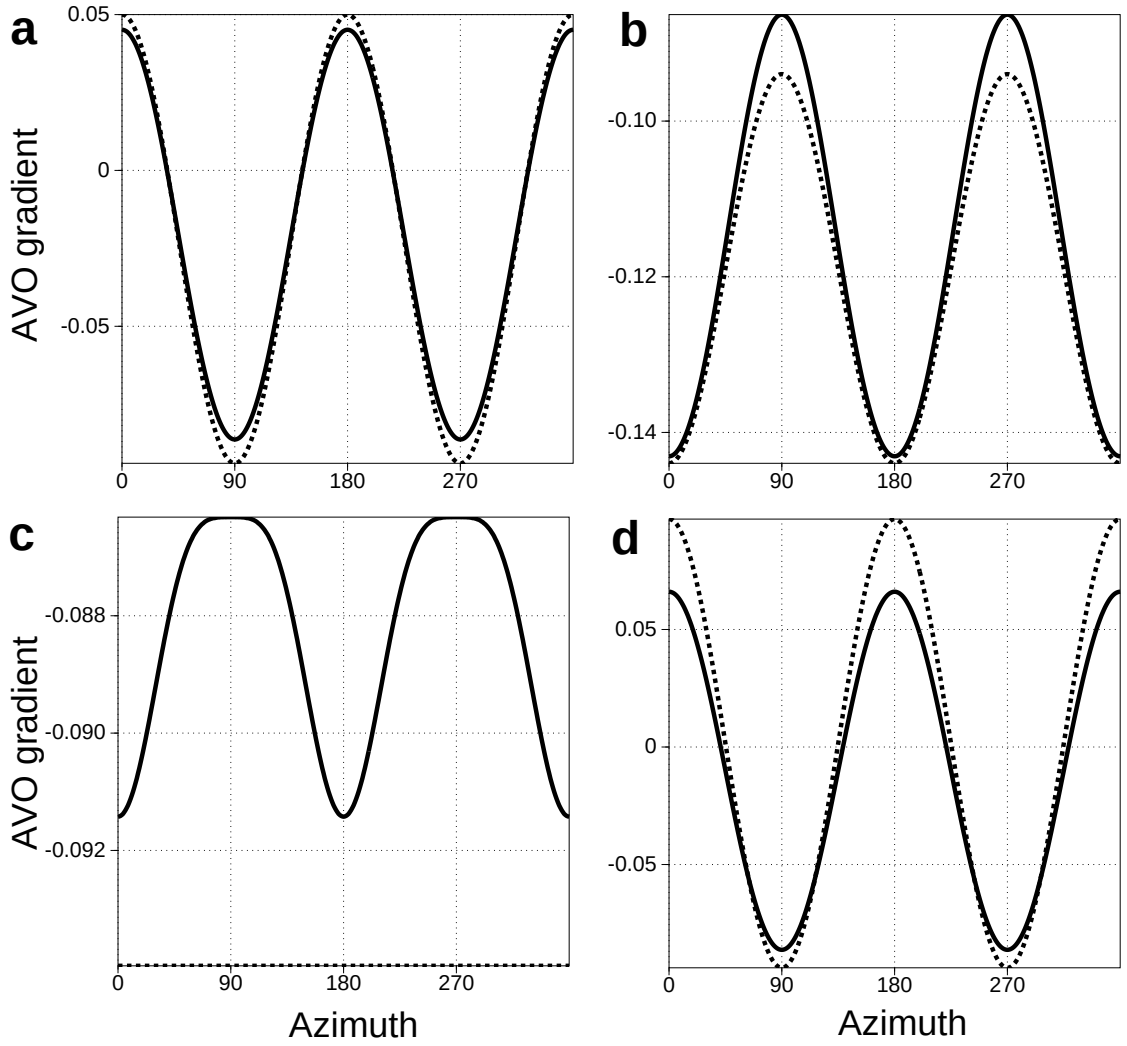


**Figure 4.** AVO gradients for an isotropic layer overlying an HTI medium as function of azimuthal phase angle. Shown are the AVO gradients extracted from the exact reflection coefficients (solid lines) and the weak elastic, weak anisotropic approximation (dashed) based on equation (8). Table 2 lists the model parameters.

plane and the isotropy-plane, respectively, and that an approximate value of $(\bar{\beta}/\bar{\alpha})$ is known. In this case, it is possible to invert for the parameter combination of $\delta^{(V)}$ and $\gamma$ in the lower medium. For example, if it is known that $\gamma$ is the only nonzero anisotropy parameter for Model a, the interpretation of the measured value of $B^{\rm ani}_{\rm observed}$ using equation (9) yields an estimated value of $\gamma_{\rm estimated} = 0.09$ as compared to the exact value of $\gamma_{\rm exact} = 0.1$. Similarly, for Model b, we would obtain a value of $\delta^{(V)}_{\rm estimated} = -0.11$ as compared to the exact solution $\delta^{(V)}_{\rm exact} = -0.1$. The azimuthal variation of the AVO gradient in Model c is very small; additionally, the azimuthal variation observed in Figure 4c correctly indicates that this change has a $\cos^4\phi$-dependence and is caused by a nonzero value of $\epsilon^{(V)}$ in the higher-angle term. Finally, if the value of $\delta^{(V)}$ is known for Model d (for example from normal-moveout analysis), $\gamma$ would be have an estimated value of $\gamma_{\rm estimated} = 0.124$ as compared to the exact value of $\gamma_{\rm exact} = 0.15$.

If $(B^{\rm iso} + B^{\rm ani})$ and $B^{\rm iso}$ are of the same sign and $(B^{\rm ani} < B)$, an alternative graphical interpretation is possible and the value of $B(\phi_k)$ can be assigned to the length of a radius vector at different azimuths $\phi_k$. The tip of this vector then delineates a curve that closely resembles an ellipse with semi-axis aligned with the symmetry-plane directions. The deviation $\triangle B \doteq \left(B(\phi_k) - B^{\rm ellipse}(\phi_k)\right)$ from the ellipse can be expressed

| | $B^{\rm ani}_{\rm observed}$ | $B^{\rm ani}_{\rm approx}$ |
|---|---|---|
| Model a | 0.131 | 0.144 |
| Model b | -0.057 | -0.05 |
| Model c | $5.4 \cdot 10^{-3}$ | 0 |
| Model d | 0.152 | 0.188 |

**Table 3.** Magnitude of the observed AVO-gradient variation and the value expected using equation (5) for the models given in Table 2.

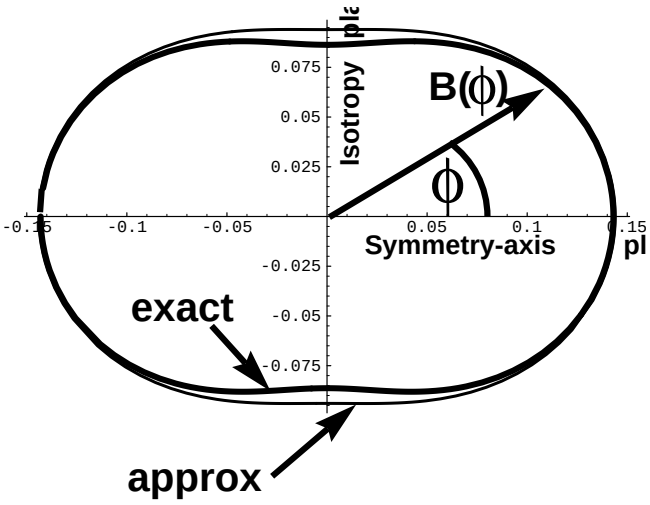


**Figure 5.** The azimuthal change in AVO gradient can often be described by an elliptically shaped curve. The curve shown here is delineated by a vector of length $B$ that has been computed for Model b in Table 2.

in the form:

$$\frac{\triangle B}{B}(\phi_k) \approx -1/2 \left(\frac{B^{\rm ani}}{B}\right)^2 \times \sin^2(\phi_k - \phi_{\rm sym}) \cos^2(\phi_k - \phi_{\rm sym}). \quad (10)$$

Equation (10) shows that the mismatch between the ellipse and the approximate AVO gradient predicted in equation (5) is a function of $B^{\rm ani}$ and $B^{\rm iso}$ and obtains its maximum value if the angle $(\phi_k - \phi_{\rm sym}) = 45°$. Under the above assumptions, fitting the azimuthally varying AVO gradient with an ellipse is therefore an accurate algorithm to determine the fracture direction and the parameter combinations $B^{\rm iso}$ and $B^{\rm ani}$. Specifically, the semi-axes will have the lengths $(B^{\rm iso})$ and $(B^{\rm iso} + B^{\rm ani})$ and point towards the symmetry-directions of the medium. Figure 5 shows one example for this approach.

There are several alternative ways to represent $R_P(i, \phi)$. For example, equation (5) can be shown to be consistent with Corrigan's (1990) approximation [equation (1)], with

$$B^{(0)} = \frac{\triangle\alpha}{\bar\alpha} - \left(\frac{2\bar\beta}{\bar\alpha}\right)^2 \left(\frac{\triangle G}{\bar G} - \triangle\gamma\right) + 1/2\, \triangle\delta^{(V)}$$
$$B^{(1)} = \left(\frac{2\bar\beta}{\bar\alpha}\right)^2 \triangle\gamma + 1/2\, \triangle\delta^{(V)}. \quad (11)$$

In exploration situations, it may happen that $\beta^\perp$, the fracture-perpendicular shear velocity is known instead of $\beta$. To achieve a higher accuracy, the AVO gradient in HTI media should then be rewritten through $\beta^\perp$:

$$B(\phi) = 1/2 \left(\frac{\triangle\alpha}{\bar\alpha} - \left(\frac{2\bar\beta^\perp}{\bar\alpha}\right)^2 \frac{\triangle G^\perp}{\bar G} + \triangle\delta^{(V)} \cos^2\phi - 2\left(\frac{2\bar\beta^\perp}{\bar\alpha}\right)^2 \triangle\gamma \sin^2\phi\right). \quad (12)$$

Finally, one of the most important lessons learned from the studies of the approximate AVO gradient is that the difference in the shear-wave splitting parameters $\triangle\gamma$ and $\triangle\delta^{(V)}$ cannot be determined separately from AVO gradient measurements in HTI media because both parameters influence the azimuthal AVO-gradient signature in the same way. Only in situations where $\delta^{(V)}$ and $\gamma$ are related (such as for tight formations) and $\bar\beta/\bar\alpha$ is known can the shear wave splitting parameter be determined directly from the azimuthal dependence of the AVO response. In all other cases, $\delta^{(V)}$ needs to be determined by independent measurements. One possibility is to relate differences in stacking velocities in the symmetry-axis plane or for a known azimuth to the vertical velocities measured in VSP experiments to $\delta^{(V)}$. Another approach is to extract $\delta^{(V)}$ from the azimuthal difference in NMO velocities (Tsvankin, 1996c).

### Azimuthal variation of the higher-angle term

For incidence angles $i > 20°$, the AVO gradient term *and* the higher-angle term will influence the reflection coefficient. For azimuths close to the symmetry axis and large incidence angles, the coefficient $\epsilon^{(V)}$ will have a significant impact on the azimuthal variations.

Here, we will discuss the interesting case of reflection coefficients with small or even nonexistent AVO gradient variations, i.e., the term $[\triangle\delta^{(V)} + 2\left(\frac{2\bar\beta}{\bar\alpha}\right)^2 \triangle\gamma]$ being negligible small. In this case, equation (5) still predicts an azimuthal change in the reflection coefficient at large angles of incidence for nonzero values of $\triangle\epsilon^{(V)}$ and $\triangle\delta^{(V)}$. Note that both parameters have a different influence on the azimuthal change of the reflection coefficient. $\triangle\delta^{(V)}$ has its major impact on the large-angle reflection response at an azimuth of 45°. $\triangle\epsilon^{(V)}$, the parameter that

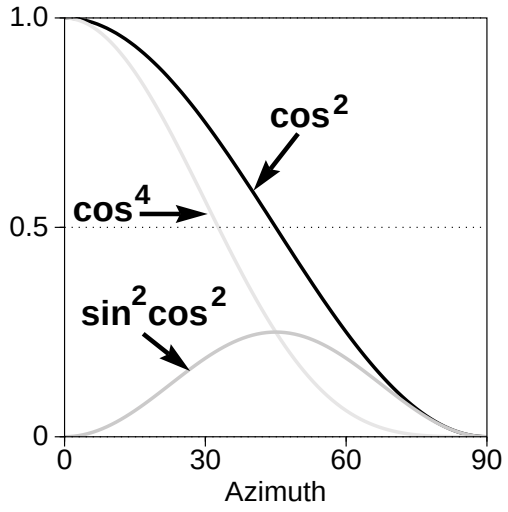


**Figure 6.** The influence of the anisotropy parameters on the reflection response depends on the azimuthal angle with the symmetry-axis plane. The AVO gradient changes as a function of the squared cosine of azimuth. The higher-angle ($\sin^2 i \tan^2 i$) term contains two parameters with different azimuthal dependences of $\cos^4\phi$ and $\sin^2\phi\cos^2\phi$.

does not have any influence on the AVO-gradient variation, is primarily responsible for the azimuthal variation of the reflection coefficient at large angles of incidence and azimuths close to the symmetry-axis direction.

The appearance of $\Delta\delta^{(V)}$ in the $\sin^2\tan^2$-term is surprising because this term does not enter the isotropy-plane coefficient (6) or the symmetry-axis plane coefficient (7). However, $\Delta\delta^{(V)}$ has only a minor impact on the azimuthal variation: at its azimuth of maximum influence (45° from the symmetry-axis plane), $\Delta\delta^{(V)}$ is scaled by $\sin^2\phi\tan^2\phi = 0.25$, which coincides with the scaling factor for $\Delta\epsilon^{(V)}$ (see Figure 6). Consequently, $\Delta\epsilon^{(V)}$ is the parameter that mostly controls the azimuthal variation.

The azimuthal AVO gradient change and the higher angular variations will often be of different sign. Specifically, assuming an isotropic overburden ($\delta_1^{(V)} = \epsilon_1^{(V)} = \gamma_1 = 0$), and a plausible inequality ($\gamma_2 > -\delta_2^{(V)}/2$) (Tsvankin, 1996c), will cause an increase of the AVO gradient for increasing azimuth. On the other hand, $\epsilon_2^{(V)}$ and $\delta_2^{(V)}$ in realistic media are negative and the $\sin^2\tan^2$-term is negative as well. Consequently, for reflections from an isotropic/HTI interface, one should expect a higher AVO gradient in the symmetry-axis plane as in the isotropy plane; in the case of azimuthally invariant AVO gradients and large incidence angles, a smaller reflection response in the symmetry-axis plane as compared to the response in the isotropy plane is more likely.

### Azimuthal variations of the transmission coefficient

A complete treatment of AVO in vertically stratified media and borehole studies in azimuthally anisotropic media include the investigation of transmission phenomena. The derivations shown in Appendix B yield the following linearized *P*-wave transmission coefficient at interfaces between two weakly anisotropic HTI media:

$$\begin{aligned} T_P(i,\phi) \;=\; & 1 - \frac{1}{2}\frac{\Delta Z}{\bar{Z}} + \\ & \frac{1}{2}\left\{\frac{\Delta\alpha}{\bar{\alpha}} + \Delta\delta^{(V)}\cos^2\phi\right\}\sin^2 i + \\ & \frac{1}{2}\left\{\frac{\Delta\alpha}{\bar{\alpha}} + \Delta\epsilon^{(V)}\cos^2\phi + \right. \\ & \left.\Delta\delta^{(V)}\sin^2\phi\cos^2\phi\right\}\sin^2 i\tan^2 i + \\ & \left\{(\Delta\epsilon^{(V)} - \Delta\delta^{(V)})\cos^2\phi\right\}\sin^4 i. \end{aligned} \qquad (13)$$

Unlike the linearized reflection coefficient, $T_P(i,\phi)$ shows no dependence on the shear-wave splitting parameter or the shear-wave vertical velocity. The difference in $\delta^{(V)}$ is the only term responsible for the azimuthal variations in the gradient term. For higher angles of incidence, two terms ($\sin^4 i$ and $\sin^2 i\tan^2 i$) with complicated azimuthal dependence of the anisotropic parameters become increasingly important.

### Orthorhombic media

HTI media are useful models to study the first-order influence of azimuthal anisotropy. More realistic models can be described by orthorhombic symmetry systems. Wave propagation in orthorhombic media is rather complex and illustrations and analysis of wavefronts and slowness surfaces in orthorhombic media can, for example, be found in (Musgrave, 1970; Helbig, 1994; Schoenberg & Helbig, 1995).

Although this investigation is valid for orthorhombic media of any origin, it is instructive to visualize an orthorhombic model as a combination of a VTI model with a system of vertical cracks such as seen in Figure 7. Also sketched in Figure 7 are the two vertical symmetry planes (symmetry plane $[x_1, x_3]$ and symmetry plane $[x_2, x_3]$). Incident waves confined to one of these symmetry planes generate just four out of the six wave modes that are created by waves incident outside of the $[x_1, x_3]$ and $[x_2, x_3]$ plane.

Let us now consider a *P*-wave incident in the $[x_2, x_3]$ plane at oblique angles with vertical. Because all four scattered modes have polarization directions parallel to

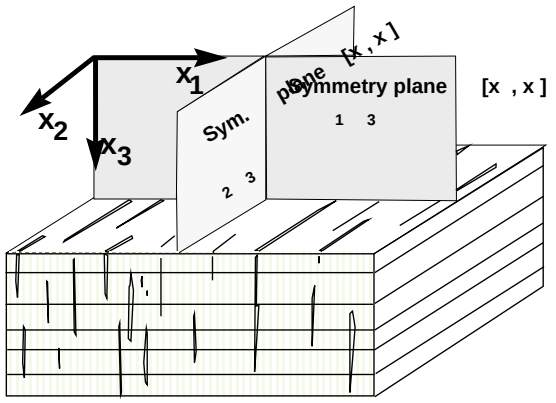


**Figure 7.** Sketch of an orthorhombic model created by combining horizontal layering with systems of vertical cracks. Also shown are the two vertical symmetry planes.

the crack planes (Figure 7), they essentially do not sense the cracks and propagate exactly as in VTI media. Consequently, reflection and transmission in the $[x_2, x_3]$ symmetry plane of orthorhombic media is analogous to the known VTI/VTI energy-partitioning problem.

The reflection problem looks more complex in the second symmetry plane $[x_1, x_3]$. Incident and generated waves are probing both the cracks and the horizontal layering and it is less straightforward to predict the structure of the scattering coefficients. However, recent studies on the analogy of HTI and VTI symmetry planes show that vertically fractured rocks can be described by an equivalent VTI medium, and it may be expected that the combination of vertical cracks and horizontal layering effectively yields a system of VTI symmetry in the $[x_1, x_3]$ plane. Based on these observations, we suggest that VTI equations are entirely valid to describe the reflection and transmission coefficients in both vertical symmetry planes of orthorhombic media.

### Analysis of symmetry-plane Christoffel systems

A more rigorous mathematical analysis of symmetry-plane reflection responses is possible by studying the corresponding Christoffel equations for orthorhombic media in the same way as shown in Rüger (1996b) for HTI models. This study (that is not repeated here) proves that the previous observations have been correct and that symmetry-plane propagation in orthorhombic media can be completely described by known VTI equations. In other words, all observations based on the equivalence of VTI and HTI media (Rüger, 1996b; Tsvankin, 1996c) remain valid for symmetry-plane propagation in orthorhombic models:

- Equations describing kinematic properties and polarizations are identical for VTI and orthorhombic models if stated in $c_{ij}$-tensor notation (and appropriate substitutions are made).
- Equations stated in Thomsen notation are identical, but the generic Thomsen parameters of the equivalent VTI model have to be replaced by parameters defined with respect to the vertical ($x_3$) axis.
- Boundary value problems such as continuity of stress and strain that are expressed in Cartesian coordinates are identical because no rotation of coordinates is necessary.

Application of these rules helps to describe seismic signatures in the $[x_1, x_3]$ plane of rocks with orthorhombic symmetry by means of already known VTI equations. Published VTI phase-velocity equations in $c_{ij}$-notation, for example, exactly expresses phase velocity in orthorhombic media. Additionally, the exact reflection and transmission coefficients for boundaries between VTI, HTI, orthorhombic and any of its combination can be computed by simply using Graebner's (1992) algorithm for VTI systems, provided that the natural coordinate frame has the same orientation on both sides of the interface.

As indicated above, a new set of Thomsen's parameters has to be introduced in the same way as previously shown for HTI media. Anticipating that a similar procedure will be necessary for the $[x_2, x_3]$ symmetry plane, a convenient notation for the equivalent VTI coefficients is (Tsvankin, 1996a)

$$\begin{aligned} \delta^{(2)} &= \frac{(c_{13}+c_{55})^2-(c_{33}-c_{55})^2}{2c_{33}(c_{33}-c_{55})} \\ \epsilon^{(2)} &= \frac{c_{11}-c_{33}}{2c_{33}}. \end{aligned}$$

Following the simple recipe of replacing $\delta$ and $\epsilon$ with $\delta^{(2)}$ and $\epsilon^{(2)}$ yields the approximate $P$-wave reflection coefficient in the $[x_1, x_3]$ symmetry-plane:

$$\begin{aligned} R_P^{[x_1,x_3]}(i) &= \frac{1}{2}\frac{\triangle Z}{\bar{Z}} + \\ &\frac{1}{2}\left(\frac{\triangle\alpha}{\bar{\alpha}} - \left(\frac{2\bar{\beta}^{\perp}}{\bar{\alpha}}\right)^2 \frac{\triangle G^{\perp}}{\bar{G}} + \triangle\delta^{(2)}\right)\sin^2 i + \\ &\frac{1}{2}\left(\frac{\triangle\alpha}{\bar{\alpha}} + \triangle\epsilon^{(2)}\right)\sin^2 i \tan^2 i\,, \end{aligned} \tag{14}$$

with $\beta^{\perp} = \sqrt{c_{55}/\rho}$. At the expense of reducing numerical accuracy, equation (14) can also be written as a function of the vertical shear-wave velocity $\beta = \sqrt{c_{44}/\rho}$ and the

well-known shear-wave splitting parameter $\gamma = \frac{c_{44}-c_{66}}{2c_{66}}$:

$$R_P^{[x_1,x_3]}(i) = \frac{1}{2}\frac{\Delta Z}{\bar{Z}} + \frac{1}{2}\left(\frac{\Delta\alpha}{\bar{\alpha}} - \left(\frac{2\bar{\beta}}{\bar{\alpha}}\right)^2\left(\frac{\Delta G}{\bar{G}} - 2\Delta\gamma\right) + \Delta\delta^{(2)}\right)\sin^2 i + \frac{1}{2}\left(\frac{\Delta\alpha}{\bar{\alpha}} + \Delta\epsilon^{(2)}\right)\sin^2 i\tan^2 i\,. \quad (15)$$

Basically the same observations can be made by comparing the $[x_2, x_3]$-plane Christoffel equations of orthorhombic and VTI media, except that the equivalence is only achieved by substituting

$$c_{11} \to c_{22}, \quad c_{55} \to c_{44}, \quad c_{13} \to c_{23}\,.$$

Hence, the $[x_2, x_3]$ plane of orthorhombic media can be described by a second equivalent VTI medium and it is possible to introduce the Thomsen parameters $\epsilon^{(1)}$ and $\delta^{(1)}$ for the $[x_2, x_3]$ plane:

$$\delta^{(1)} = \frac{(c_{23}+c_{44})^2 - (c_{33}-c_{44})^2}{2c_{33}(c_{33}-c_{44})}$$

$$\epsilon^{(1)} = \frac{c_{22}-c_{33}}{2c_{33}}\,.$$

Finally, substitution of $\delta^{(1)}$ and $\epsilon^{(1)}$ yields the approximate reflection coefficient for the $[x_2, x_3]$ symmetry plane:

$$R_P^{[x_2,x_3]}(i) = \frac{1}{2}\frac{\Delta Z}{\bar{Z}} + \frac{1}{2}\left(\frac{\Delta\alpha}{\bar{\alpha}} - \left(\frac{2\bar{\beta}}{\bar{\alpha}}\right)^2\frac{\Delta G}{\bar{G}} + \Delta\delta^{(1)}\right)\sin^2 i + \frac{1}{2}\left(\frac{\Delta\alpha}{\bar{\alpha}} + \Delta\epsilon^{(1)}\right)\sin^2 i\tan^2 i\,. \quad (16)$$

The introduction of the set of new Thomsen parameters $(\delta^{(1)}, \delta^{(2)}, \epsilon^{(1)}, \epsilon^{(2)})$ has advantages not only for the study of reflection coefficient, but is generally useful in describing seismic signatures within and outside of the symmetry planes (Tsvankin, 1996a). To completely describe orthorhombic symmetry systems, we need a total of seven anisotropy coefficients together with two vertical velocities to replace the nine independent coefficients in the orthorhombic stiffness matrix. One choice of anisotropy parameters is shown in Table 4, together with their relation to the generic Thomsen parameters and parameters $\delta^{(V)}$ and $\epsilon^{(V)}$ introduced for HTI models. A more detailed discussion of effective parameters in orthorhombic media is out of the scope of this paper and is presented in Tsvankin (1996a).

### Azimuthal variation of orthorhombic reflection coefficients

The discussion above shows that the approximate reflection coefficients in the two vertical symmetry planes of orthorhombic media are identical to the HTI symmetry-axis plane reflection coefficient. This result makes it possible to use the difference in $P$-wave reflection coefficients in the two vertical symmetry planes of orthorhombic media in the inversion for the shear-wave splitting parameter. To eliminate the "isotropic quantities" in equations (15) and (16), I follow the approach suggested by Rüger and Tsvankin (1995) of taking the difference between the two coefficients:

$$R_P^{[x_1,x_3]} - R_P^{[x_2,x_3]} = \left\{\left(\frac{2\bar{\beta}}{\bar{\alpha}}\right)^2\Delta\gamma_2 + \frac{1}{2}\left(\Delta\delta^{(2)} - \Delta\delta^{(1)}\right)\right\}\sin^2 i + \frac{1}{2}\left\{\Delta\epsilon^{(2)} - \Delta\epsilon^{(1)}\right\}\sin^2 i\tan^2 i\,. \quad (17)$$

For an isotropic overburden, equation (17) shows that the difference in the AVO gradient depends on just three anisotropic parameters - the shear-wave splitting parameter $\gamma_2$ and two new parameters $\delta_2^{(1)}$ and $\delta_2^{(2)}$ describing the anisotropy for near-vertical $P$-wave propagation in the symmetry planes. Tsvankin (1996a) shows that it is possible to obtain the $\delta^{(1)}$ and $\delta^{(2)}$ parameters from short-spread $P$-wave moveout analysis in the vertical symmetry planes combined with an estimate of the vertical velocity; alternatively, these parameters can be estimated by the difference between the stacking velocities and the vertical velocities measured in a VSP experiment.

The approximate (low angle) reflection coefficient for an isotropic overburden and a reflecting orthorhombic layer has been derived by Corrigan (1990). Represented

| Orthorhombic | VTI | HTI |
|---|---|---|
| $\delta^{(2)} = \frac{(c_{13}+c_{55})^2-(c_{33}-c_{55})^2}{2c_{33}(c_{33}-c_{55})}$ | $\delta$ | $\delta^{(V)}$ |
| $\delta^{(1)} = \frac{(c_{23}+c_{44})^2-(c_{33}-c_{44})^2}{2c_{33}(c_{33}-c_{44})}$ | $\delta$ | 0 |
| $\delta^{(3)} = \frac{(c_{12}+c_{66})^2-(c_{11}-c_{66})^2}{2c_{11}(c_{11}-c_{66})}$ | 0 | $\delta^{(V)} - 2\epsilon^{(V)}$ |
| $\epsilon^{(2)} = \frac{c_{11}-c_{33}}{2c_{33}}$ | $\epsilon$ | $\epsilon^{(V)}$ |
| $\epsilon^{(1)} = \frac{c_{22}-c_{33}}{2c_{33}}$ | $\epsilon$ | 0 |
| $\gamma^{(2)} = \frac{c_{66}-c_{44}}{2c_{44}}$ | $\gamma$ | $-\gamma$ |
| $\gamma^{(1)} = \frac{c_{66}-c_{55}}{2c_{55}}$ | $\gamma$ | 0 |

**Table 4.** Seven anisotropy parameters (plus two vertical velocities) completely describe orthorhombic anisotropy. Their relations to the generic (VTI) Thomsen coefficients and to HTI parameters $\delta^{(V)}$ and $\epsilon^{(V)}$ are shown in the second and third column. The relation for $\delta^{(3)}$ and $\gamma^{(2)}$ are approximate, the other relations are valid for any strength of anisotropy.

in the new parameterization, his solution implies the following form of the approximate low-angle reflection coefficient for arbitrary azimuth

$$R_P(i,\phi) = \frac{1}{2}\frac{\Delta Z}{\bar{Z}} + \frac{1}{2}\left\{\frac{\Delta\alpha}{\bar{\alpha}} - \left(\frac{2\bar{\beta}}{\bar{\alpha}}\right)^2 \frac{\Delta G}{\bar{G}} + \left[\delta_2^{(2)} + 2\left(\frac{2\bar{\beta}}{\bar{\alpha}}\right)^2 \gamma_2\right]\cos^2\phi + \delta_2^{(1)}\sin^2\phi\right\}\sin^2 i\ . \tag{18}$$

## Discussion and conclusions

Analysis of reflection coefficients in azimuthally anisotropic media shows that the magnitude and the functional type of the azimuthal variation of *P*-wave reflectivity can be inverted for the anisotropy parameters and the symmetry-plane directions of the subsurface.

The examples shown in this paper show that the derived approximate reflection coefficients closely describe the exact reflection response. However, rather than achieving a high numerical accuracy with the new approximations, it is more important in this study to establish a physical foundation for (exact) numerical inversion algorithms and create simple dependencies that interpreters can use to quickly evaluate the importance of anisotropy for their project. To obtain a reasonably simple representation of the otherwise incomprehensibly complex reflection coefficients, a perturbation approach has been used in the derivation. The main assumption in this reflection-coefficient study - small jumps in the elastic parameters across the reflecting interface and weak anisotropy - are geologically reasonable and proved useful in many exploration contexts. Although the approximations may help to detect pronounced anomalies, they fail in any quantitative analysis at interfaces with a large contrast in the elastic parameters and strong anisotropy. The HTI approximations shown will also be inaccurate if the natural coordinate systems of the incidence and reflected layer differ significantly in orientation, i.e., when the axis of symmetry changes abruptly across the boundary.

Within the limits of these assumptions, the approximate *P*-wave reflection coefficient for HTI interfaces predicts a change of the AVO gradient as a function of the squared cosine of azimuth. This change can be inverted for the symmetry-plane directions and a combination of the shear-wave splitting parameter $\gamma$ and the anisotropy coefficient $\delta^{(V)}$. Coefficients $\gamma$ and $\delta^{(V)}$ cause the same functional form of the azimuthal variation in the AVO gradient and cannot be extracted individually.

The two symmetry-plane directions can even be extracted in situations where no azimuthal AVO-gradient change can be observed. In this case, the azimuthal variation at large incidence angles is primarily dependent on the anisotropy coefficient $\epsilon^{(V)}$ (closely related to Thomsen's parameter $\epsilon$) and provides enough information to detect the natural coordinate system of the subsurface.

Certainly, realistic models of fractured reservoirs deviate from simple HTI media, and it is interesting whether the reflection response in media of lower symmetry differs significantly from that in the HTI case. This study shows that although wave propagation is significantly more complex in orthorhombic media, the approximate reflection coefficient basically has the same form as in HTI models. The main observation of the study of reflection coefficients in orthorhombic media is that the difference between the *P*-wave reflection response in the vertical symmetry-planes is a function of the shear-wave splitting parameter $\gamma$ and two new parameters describing the anisotropy for near-vertical *P*-wave propagation in the symmetry planes.

The practical implementation of the newly proposed AVO inversion faces challenges similar or even greater than for conventional AVO analysis. Prerequisite for any useful AVO-with-azimuth investigation is a proper processing sequence that preserves azimuthally varying amplitude signatures. Moreover, a profound understanding of lateral inhomogeneities is required. Wave propagation in an anisotropic overburden has a significant impact on the amplitude variations with offset and azimuth (Tsvankin, 1995; Rüger & Tsvankin, 1995) and need to be included in any meaningful AVO analysis. Other difficulties include thin layering, curved reflectors or dipping symmetry-axes. These issues are not within the scope of this investigation; however, they will be addressed in a forthcoming paper on AVO for fractured reservoirs.

## Acknowledgments

Thanks to Ilya Tsvankin for guidance, discussions and support. Vladimir Grechka reviewed this manuscript and Björn Rommel examined Appendix A. Dennis Corrigan was kind enough to share his programs, derivations and time. Jack Cohen's *Mathematica*-package ATools.m was very helpful in the derivation of the linearized reflection coefficient. Thanks also to Leon Thomsen for pointing out the original author of approximation (6) and to members of the A(nisotropy)-Team at the Center for Wave Phenomena (CWP) for useful discussions. The support for this work was provided by the members of the Consortium Project on Seismic Inverse Methods for Complex Structures at CWP, Colorado School of Mines, and by the United States Department of Energy (project "Velocity

Analysis, Parameter Estimation, and Constraints on Lithology for Transversely Isotropic Sediments" within the framework of the Advanced Computational Technology Initiative). Partial funding for this project has also been provided by a scholarship from Phillips Petroleum Co. and by a grant from Coleman Energy & Environmental Systems- Blackhawk Geoscience Division.

## References

Aki, K., & Richards, P. G. 1980. *Quantitative seismology: Theory and methods.* W. N. Freeman & Co.

Alford, R. M. 1986. Shear data in the presence of azimuthal anisotropy: Dilley, Texas. *In: 56th Annual Internat. Mtg., Soc. Expl. Geophys., Expanded Abstracts.* Soc. Expl. Geophys.

Banik, N. C. 1987. An effective anisotropy parameter in transversely isotropic media. *Geophysics*, **52**(12), 1654–1664.

Bortfeld, R. 1961. Approximation to the reflection coefficients of plane longitudinal and transverse waves. *Geophysical Prospecting*, **9**, 485–502.

Corrigan, D. 1990. The effect of azimuthal anisotropy on the variation of reflectivity with offset. *In: 4IWSA.* Soc. Expl. Geophys.

Crampin, Stuart. 1985. Evidence for aligned cracks in the Earth's crust. *First Break*, **3**, 12–15.

Graebner, M. 1992. Plane-wave reflection and transmission coefficients for a transversely isotropic solid (short note). *Geophysics*, **57**(11), 1512–1519.

Helbig, K. 1994. *Foundations of anisotropy for exploration seismics.* Handbook of Geophysical Exploration, vol. 22. Elsevier Science Inc.

Johnson, W. E. 1995. Direct detection of gas in pre-Tertiary sediments? *The Leading Edge*, **14**(2), 119–122.

Koefoed, O. 1955. On the effect of Poisson's ratio of rock strata on the reflection coefficients of plane waves. *Geophysical Prospecting*, **3**, 381–387.

Lynn, H. B. et al. 1995. The effects of azimuthal anisotropy in P-wave 3-D seismic. *In: 65th Annual Internat. Mtg., Soc. Expl. Geophys., Expanded Abstracts.* Soc. Expl. Geophys.

Mallick, S. 1995. *personal communication.*

Mallick, S., & Fraser, L. N. 1991. Reflection/transmission coefficients and azimuthal anisotropy in marine studies. *Geo. J. Int.*, **105**, 241–252.

Martin, M. A., & Davis, T. L. 1987. Shear-wave birefringence - a new tool for evaluating fractured reservoirs. *The Leading Edge*, **6**(10), 22–28.

Michelena, R. J. 1995. Quantifying errors in fracture orientation estimated from surface P-S converted waves. *In: 65nd Annual Internat. Mtg., Soc. Expl. Geophys., Expanded Abstracts.* Soc. Expl. Geophys.

Musgrave, M. J. P. 1970. *Crystal acoustics.* Holden Day, San Francisco.

Richards, P. G., & Frasier, C. W. 1976. Scattering of elastic waves from depth-dependent inhomogeneities. *Geophysics*, **41**(3), 441–458.

Rommel, B.E. 1994. Approximate polarization of plane waves in a medium having weak transverse isotropy. *Geophysics*, **59**, 1605–1612.

Rüger, A. 1996a. Analytic insight into shear-wave AVO for fractured reservoirs. *in Center for Wave Phenomena report CWP-202.*

Rüger, A. 1996b. P-wave reflection coefficients for transversely isotropic models with vertical and horizontal axis of symmetry. *Geophysics, submitted.*

Rüger, A., & Tsvankin, I. 1995. Azimuthal variation of AVO response for fractured reservoirs. *Pages 1103–1106 of: 65th Annual Internat. Mtg., Soc. Expl. Geophys., Expanded Abstracts*, vol. 95.

Schoenberg, M., & Helbig, K. 1995. Orthorhombic media: Modeling elastic wave behavior in a vertically fractured Earth. *Geophysics, in print.*

Thomsen, L. 1986. Weak elastic anisotropy. *Geophysics*, **51**(10), 1954–1966.

Thomsen, L. 1988. Reflection seismology over azimuthally anisotropic media. *Geophysics*, **53**(3), 304–313.

Thomsen, L. 1993. Weak anisotropic reflections. *In Offset Dependent Reflectivity (Castagna and Backus, Eds.), SEG, Tulsa.*

Thomsen, L. 1995. Elastic anisotropy due to aligned cracks in porous rock. *Geophysical Prospecting*, **43**, 805–829.

Thomsen, Leon. 1990. Poisson was not a geophysicist. *The Leading Edge*, **9**(12), 27–29.

Tsvankin, I. 1995. Body-wave radiation patterns and AVO in transversely isotropic media. *Geophysics*, **60**(5), 1409–1425.

Tsvankin, I. 1996a. Effective parameters and reflection seismic signatures for orthorhombic anisotropy. *in Center for Wave Phenomena report CWP-199.*

Tsvankin, I. 1996b. *P*-wave signatures and notation for transversely isotropic media: An overview. *Geophysics*, **61**(2), 467–483.

Tsvankin, I. 1996c. Reflection moveout and parameter estimation for horizontal transverse isotropy. *Geophysics, accepted.*

Ursin, B., & Haugen, G. 1996. Weak-contrast approximation of the elastic scattering matrix in anisotropic media. *Proceedings of workshop on seismic waves in laterally inhomogeneous media, Castle of Trest,*

*Czech Republic, accepted.*

Winterstein, D.F. 1990. Velocity anisotropy terminology for geophysicists. *Geophysics*, **55**, 1070–1088.

Wright, J. 1986. Reflection coefficients at pore-fluid contacts as a function of offset (short note). *Geophysics*, **51**(9), 1858–1860.

Yardley, G. S.; Graham, G., & Crampin, S. 1991. Viability of shear-wave amplitude versus offset studies in anisotropic media. *Geophys. J. Int.*, **107**, 493–503.

## APPENDIX A: Polarization vectors in HTI media

One of the key elements to solve reflection and transmission coefficients in anisotropic media is the derivation of polarization vectors. Equations describing the direction of compressional wave polarizations in VTI media have been published by Rommel (1994) and Tsvankin (1996b). Denoting the phase and polarization angles with the symmetry axis as $\theta$ and $\gamma$, respectively, one can show that

$$\begin{aligned} \cos\gamma &= \left(1 - f\,\sin^2\theta\,[\,\delta + 2(\epsilon-\delta)\sin^2\theta\,]\right)\cos\theta \\ \sin\gamma &= \left(1 + f\,\cos^2\theta\,[\,\delta + 2(\epsilon-\delta)\sin^2\theta\,]\right)\sin\theta \end{aligned} \quad \text{(A1)}$$

with $f = \alpha^2/(\alpha^2-\beta^2)$.

Polarization vectors in HTI media can be derived using the analogy between VTI and HTI media (Rüger, 1996b). First, replace Thomsen's (1986) parameters $\epsilon$ and $\delta$ with $\epsilon^{(V)}$ and $\delta^{(V)}$, the parameters of the equivalent VTI model. This substitutions yield the polarization vector for quasi $P$-waves in the vertical plane containing the symmetry axis of HTI media and, as seen below, provides sufficient information to determine the polarization for $P$-waves with any incidence and azimuthal angle.

Equation A1, expressed in terms of angles $\gamma'$ and $\theta'$ with respect to the horizontal symmetry axis in HTI models yields

$$\begin{aligned} \sin\gamma' &= \left(1 - f\,\cos^2\theta'\,[\,\delta^{(V)} + 2(\epsilon^{(V)}-\delta^{(V)})\cos^2\theta'\,]\right)\sin\theta' \\ &= \mathrm{m}(\theta')\sin\theta' \\ \cos\gamma' &= \left(1 + f\,\sin^2\theta'\,[\,\delta^{(V)} + 2(\epsilon^{(V)}-\delta^{(V)})\cos^2\theta'\,]\right)\cos\theta' \\ &= \mathrm{l}(\theta')\cos\theta', \end{aligned} \quad \text{(A2)}$$

where $f = \alpha^2/(\alpha^2-\beta^2)$ as in equation (A1), but $\alpha$ and $\beta$ denote the vertical compressional and the vertical fracture-parallel shear-wave velocity, respectively.

Physical properties in transversely isotropic media are invariant for a fixed angle with the symmetry axis, hence it is perfectly valid to generalize this equation and allow the polarization vector to rotate about the horizontal axis. The next step in the derivation of the polarization vectors is to relate the angles $\gamma'$ and $\theta'$ with the symmetry axis to their corresponding incidence angle and azimuth. From simple geometry (Figure A1), we can find a relation between the cosine of an arbitrary angle $\alpha$ with the horizontal axis and its associated incidence polar angle $i$ and azimuth $\phi$:

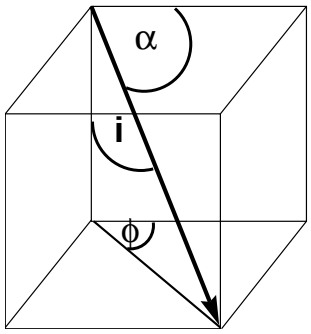


**Figure A1.** Relation between an arbitrary angle with the horizontal axis $\alpha$ and its associated incidence angle $i$ and azimuth $\phi$.

$$\cos\alpha = \sin i\,\cos\phi\,. \quad \text{(A3)}$$

The cartesian components of the unit polarization vector $\hat{\mathrm{d}} = (d_1, d_2, d_3)^T$ and the unit wave vector $\hat{\mathrm{n}} = (n_1, n_2, n_3)^T$ normal to the wavefront can be written as

$$\hat{\mathrm{d}} = \begin{pmatrix} \sin i_\mathrm{d}\,\cos\phi_\mathrm{d} \\ \sin i_\mathrm{d}\,\sin\phi_\mathrm{d} \\ \cos i_\mathrm{d} \end{pmatrix} \qquad \hat{\mathrm{n}} = \begin{pmatrix} \sin i\,\cos\phi \\ \sin i\,\sin\phi \\ \cos i \end{pmatrix}. \quad \text{(A4)}$$

Here, angles of the polarization vector and the phase vector with the vertical axis are called $i_\mathrm{d}$ and $i$, respectively; similar notation applies to the azimuthal angles.

Using equations (A2) and (A3), one can relate the first components to obtain the simple expression $d_1 = \mathrm{l}\,n_1$. Corresponding equations for the two remaining components can be found using geometrical observations. First note that in transversely isotropic media, the polarization vector $\hat{\mathrm{n}}$ lies in the plane formed by the symmetry axis and the phase vector. The two triangles shown in Figure A2 thus have the same angle $\psi$ and we find

$$\begin{aligned} d_2 = \overline{A'B'} &= \sin\gamma'\,\cos\psi \\ &= n_2\,\frac{\sin\gamma'}{\sin\theta'} \\ &= \mathrm{m}\,n_2 \\ d_3 = \overline{B'C'} &= \sin\gamma'\,\sin\psi \\ &= n_3\,\frac{\sin\gamma'}{\sin\theta'} \\ &= \mathrm{m}\,n_3\,. \end{aligned} \quad \text{(A5)}$$

Summarizing, we see that the $P$-wave polarization vec-

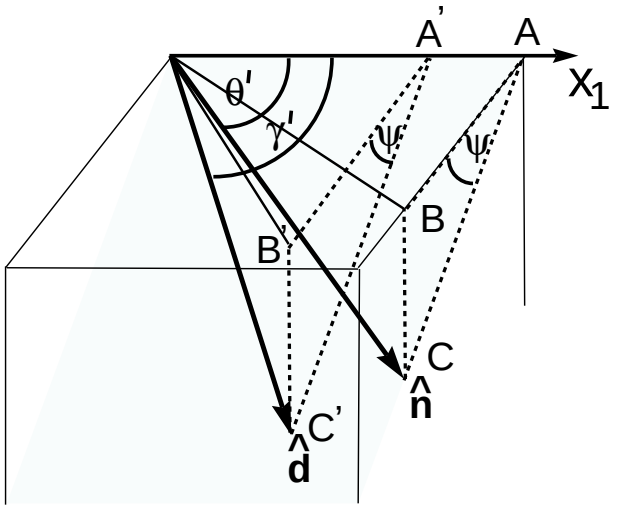


**Figure A2.** Phase vector n̂ and polarization vector d̂ lie in a common plane with the symmetry axis $x_1$. Angle $\psi$ is identical for triangles $\triangle$ABC and $\triangle A'B'C'$.

tor in HTI media can be expressed as function of the incidence and azimuthal phase angle as

$$\hat{\mathrm{d}}\,(i,\phi) = \begin{pmatrix} \mathrm{l}(i,\phi)\,\sin i\,\cos\phi \\ \mathrm{m}(i,\phi)\,\sin i\,\sin\phi \\ \mathrm{m}(i,\phi)\,\cos i \end{pmatrix}, \tag{A6}$$

where l and m (equation (A2)) are given as

$$\begin{aligned} \mathrm{m}(i,\phi) &= 1 - f\,\sin^2 i\cos^2\phi\,\times \\ &\quad [\delta^{(V)} + 2(\epsilon^{(V)} - \delta^{(V)})\sin^2 i\cos^2\phi] \\ \mathrm{l}(i,\phi) &= 1 + f\,(1 - \sin^2 i\cos^2\phi)\,\times \\ &\quad [\delta^{(V)} + 2(\epsilon^{(V)} - \delta^{(V)})\sin^2 i\cos^2\phi]\,. \end{aligned}$$

Although the shear wave polarizations are not necessary for this study, they can be derived using equation (A6). Note that quasi-compressional and shear wave polarizations are mutually orthogonal, with the $S^{\|}$ wave being a truly transverse mode ($\hat{d}^{S^{\|}} \perp \hat{n}$) with the polarization vector confined to the isotropy plane.

## APPENDIX B: Derivation of azimuthally varying approximate reflection coefficients in HTI media

Here, the derivation of approximate reflection and transmission coefficients for interfaces between VTI layers (Thomsen, 1993) is extended to azimuthally anisotropic HTI media. The approximations are derived for a boundary between two weakly anisotropic media with the same symmetry-axis direction and for small discontinuities in elastic properties across the boundary. Due to the considerable size of the matrices and vectors considered in this derivation, it is impossible to explicitly state all quantities used in this appendix. However, I outline each step of the derivation in detail and provide all information necessary to reproduce the final result.

The main idea of the derivation is to replace the exact boundary value problem

$$\mathbf{A}\,\mathbf{R} = \mathbf{b}\,, \tag{B1}$$

where $\mathbf{A}$ is the boundary equation matrix formed by the scattered (reflected and transmitted) wave types, $\mathbf{R}$ is the vector of reflection and transmission coefficients, and $\mathbf{b}$ is composed of the contribution of the incident wave to the boundary conditions, with a perturbation from the corresponding expression for the interface between two identical, isotropic and homogeneous media. Denoting the unperturbed quantities with the superscript $\mathbf{u}$, Thomsen (1993) showed that

$$\mathbf{\Delta R} = \left(\mathbf{A^u}\right)^{-1}\left(\mathbf{\Delta b} - \mathbf{\Delta A}\,\mathbf{R^u}\right)\,. \tag{B2}$$

Here, the operator $\mathbf{\Delta}$ is defined as $\mathbf{\Delta} \equiv d_j \frac{\partial}{\partial d_j}$ with the vector $d_j$ of small deviations from the two identical homogeneous, isotropic media given by

$$d_j = (\frac{\triangle\alpha}{\bar{\alpha}}, \frac{\triangle\beta}{\bar{\beta}}, \frac{\triangle\rho}{\bar{\rho}}, \delta_1^{(V)}, \delta_2^{(V)}, \epsilon_1^{(V)}, \epsilon_2^{(V)}, \gamma_1, \gamma_2)^T\,. \tag{B3}$$

The $6 \times 6$ matrix $\mathbf{A^u}$ needs to be inverted analytically. This can be achieved by relating $\mathbf{A^u}$ to the eigenvectors of the transformed wave equation (Ursin & Haugen, 1996). To find the elements $\mathbf{\Delta b}$ and $\mathbf{\Delta A}$, it is necessary to use the weak anisotropy approximations to polarization vectors and phase velocities shown in the main text [equations (3) and (4)], while the approximate refracted angles can be derived using Snell's law. The two elements of $\mathbf{\Delta R}$ of most interest are the $P$-wave reflection and transmission coefficients shown in equation (5) and (13).

## APPENDIX C: Approximate symmetry-axis plane scattering coefficients for HTI/HTI interfaces

The following equations are accurate for small discontinuities in the elastic properties across the boundary and weak anisotropy. The medium considered has the same parameterization as introduced in the main text. $R_P$ and $T_P$ are the $P$-wave reflection and transmission coefficients. Similar notation is used for the shear-wave scattering coefficients of $S^{\|}$ and $S^{\perp}$, polarized parallel and perpendicular to the isotropy plane, respectively.

To facilitate the comparison with the reflection coefficient in the isotropy plane, the approximations are

shown as functions of $\beta$, the vertical velocity of the shear mode polarized parallel to the isotropy plane.

For cases where the best possible linear approximation of the symmetry-axis scattering coefficient is desired, the coefficient should be rewritten as function of the shear velocity $\beta^{\perp}$ ($\approx \beta(1-\gamma)$).

A detailed discussion of the $P$-wave approximations is given in the main text. The shear-wave reflection coefficients are thoroughly investigated in Rüger (1996a).

$$
\begin{aligned}
R_P(i) &= \frac{1}{2}\frac{\Delta Z}{\bar{Z}} + \\
&\quad \frac{1}{2}\left\{\frac{\Delta\alpha}{\bar{\alpha}} - \left(\frac{2\bar{\beta}}{\bar{\alpha}}\right)^2\left(\frac{\Delta G}{\bar{G}} - 2\Delta\gamma\right) + \right. \\
&\quad \left.\Delta\delta^{(V)}\right\}\sin^2 i + \\
&\quad \frac{1}{2}\left(\frac{\Delta\alpha}{\bar{\alpha}} + \Delta\epsilon^{(V)}\right)\sin^2 i\tan^2 i \\
T_P(i) &= 1 - \frac{1}{2}\frac{\Delta Z}{\bar{Z}} + \\
&\quad \left(\Delta\epsilon^{(V)} - \Delta\delta^{(V)}\right)\sin^4 i + \\
&\quad \frac{1}{2}\left(\frac{\Delta\alpha}{\bar{\alpha}} + \Delta\delta^{(V)}\right)\sin^2 i + \\
&\quad \frac{1}{2}\left(\frac{\Delta\alpha}{\bar{\alpha}} + \Delta\epsilon^{(V)}\right)\sin^2 i\tan^2 i \\
R_{S^\perp}(j) &= -\frac{1}{2}\left(\frac{\Delta\rho}{\bar{\rho}} + \frac{\Delta\beta}{\bar{\beta}} - \Delta\gamma\right) + \\
&\quad \left\{\frac{7}{2}\left(\frac{\Delta\beta}{\bar{\beta}} - \Delta\gamma\right) + 2\frac{\Delta\rho}{\bar{\rho}} - \right. \\
&\quad \left.\frac{1}{2}\left(\frac{\bar{\alpha}}{\bar{\beta}}\right)^2(\Delta\delta^{(V)} - \Delta\epsilon^{(V)}\right\}\sin^2 j \\
&\quad -1/2\left(\frac{\Delta\beta}{\bar{\beta}} - \Delta\gamma\right)\sin^2 j\tan^2 j \\
T_{S^\perp}(j) &= 1 - \frac{1}{2}\left(\frac{\Delta\rho}{\bar{\rho}} + \frac{\Delta\beta}{\bar{\beta}} - \Delta\gamma\right) + \\
&\quad \left(\frac{\bar{\alpha}}{\bar{\beta}}\right)^2\left(\Delta\delta^{(V)} - \Delta\epsilon^{(V)}\right)\sin^4 j + \\
&\quad \frac{1}{2}\left\{\frac{\Delta\beta}{\bar{\beta}} - \Delta\gamma + \frac{1}{2}\left(\frac{\bar{\alpha}}{\bar{\beta}}\right)^2 \times \right. \\
&\quad \left.(\Delta\epsilon^{(V)} - \Delta\delta^{(V)})\right\}\sin^2 j + \\
&\quad \left(\frac{\Delta\beta}{\bar{\beta}} - \Delta\gamma\right)\sin^2 j\tan^2 j \\
R_{S^\parallel}(j) &= -\frac{1}{2}\left(\frac{\Delta\rho}{\bar{\rho}} + \frac{\Delta\beta}{\bar{\beta}}\right) + \\
&\quad \frac{1}{2}\left(\frac{\Delta\beta}{\bar{\beta}} - \Delta\gamma\right)\sin^2 j + \\
&\quad \frac{1}{2}\left(\frac{\Delta\beta}{\bar{\beta}} - \Delta\gamma\right)\sin^2 j\tan^2 j \\
T_{S^\parallel}(j) &= 1 + R_{S^\parallel}(j)\,.
\end{aligned}
$$